Analysis of the high-frequency performance of InGaAs/InAlAs nanojunctions using a three-dimensional Monte Carlo simulator

T. Sadi, Jean-Luc Thobel

Analysis of the high-frequency performance of InGaAs / InAlAs nanojunctions using a three-dimensional Monte Carlo simulator

Cite as: J. Appl. Phys. **106**, 083709 (2009); https://doi.org/10.1063/1.3248358
Submitted: 06 May 2009 • Accepted: 21 September 2009 • Published Online: 26 October 2009

Toufik Sadi and Jean-Luc Thobel

Analysis of the high-frequency performance of InGaAs/InAlAs nanojunctions using a three-dimensional Monte Carlo simulator

Toufik Sadi[a] and Jean-Luc Thobel
Institut d'Electronique, de Microélectronique et de Nanotechnologie (IEMN), UMR-CNRS 8520, Université Lille 1, 59652 Villeneuve d'Ascq Cédex, France

(Received 6 May 2009; accepted 21 September 2009; published online 26 October 2009)

We report results from the investigation of the intrinsic high-frequency (HF) behavior of three-terminal junctions based on InGaAs/InAlAs heterostructures, using a well-calibrated three-dimensional semiclassical ensemble Monte Carlo simulation model. The simulator incorporates a more realistic surface charge model, designed specifically for HF simulations. A full analysis of the dynamics of electron transport in the devices is performed and a prediction of its intrinsic HF performance is presented. Simulation results demonstrate how these devices may be suitable for applications in the terahertz frequency range. Most importantly, we illustrate the important role played by surface charge effects in this frequency regime. The necessity of considering these effects as a key design factor for the development of future nanojunction structures operating in the terahertz regime is therefore discussed. © *2009 American Institute of Physics*. [doi:10.1063/1.3248358]

I. INTRODUCTION

The miniaturization of semiconductor devices to allow an increased packing density and hence functionality of integrated circuits led to great advances in the electronics industry, allowing faster and more sophisticated electronic products to be commercialized. State-of-the-art devices are approaching the nanoscale range, and the sustainment of the traditional scaling methods, by maintaining the devices basic structure while shrinking its size, faces increasing technological roadblocks and fundamental challenges. In this case, further improvement of performance should not be expected from size reduction but rather from profound change in geometry. Progress in nanolithography led to the development of complex-geometry devices such as FinFETs, gate all around Field-Effect Transistors (FETs), and ballistic switches. Moreover, recent advances in "bottom-up" techniques have considerably expanded the range of possibilities in device fabrication, as illustrated by the successful realization of a wide variety of nanowires. In this context, the development of reliable three-dimensional (3D) simulation tools are essential in order to help designers to determine the best structures. These simulators are also important for providing insight into the physical behavior of nanostructures which is still not completely understood, especially at high frequencies, for which most nanodevices are designed.

Semiconductor nanojunctions (also referred to as ballistic switches) based on III-As heterojunctions are a good example of several innovative designs aiming at extending the limits of traditional scaling. Such complex-geometry quasiballistic (low-scattering) nanodevices have attracted substantial attention in recent years, due to their nonlinear properties, which are not observed in classical (diffusive) devices. A great number of theoretical and experimental studies[1–6] focused on nanojunctions based on InGaAs channels with high indium (In) contents ($>50\%$). The high electron velocity in such channels reduces the electron transit time, opening the possibility of using such devices, for example, for data processing at ultrahigh bit rate. The compatibility of InGaAs-based ballistic devices with modern HEMT technology offers an additional advantage; the integration of InGaAs-based High-Electron Mobility Transistors (HEMTs), which are already operational in the millimeter frequency range, with these quasiballistic devices may result in extending device operation to the terahertz regime.

Semiconductor nanojunctions based on InGaAs channels are intended for HF applications, and therefore a thorough analysis of their behavior at these conditions is necessary for providing full insight into their operation. This work concerns the theoretical investigation of electron transport and surface charge effects in three-terminal T-branch junctions (TBJs) at high frequencies, by using a well-established 3D semiclassical ensemble Monte Carlo simulator.[7] Three-terminal junctions are emerging devices that can be used for multiple purposes. Studies showed that the structures can function as voltage rectifiers,[8] diodes,[9] and triodes,[10] and can be incorporated as building blocks in electronic devices and circuits.[11] As thoroughly discussed in the authors' previous work,[7] 3D models are more suitable for a realistic simulation of transport properties in nanojunctions, as compared to two-dimensional (2D) models, in spite of the increased computational cost involved.

The fundamental functioning of TBJs depends strongly on the improved electron transport in the junction. For this reason, TBJs are usually fabricated on high mobility heterostructures (as explained above), with the junction-region size being comparable to the mean free path of the 2D electron gas. Injected electrons entering the active region of the device do not lose their kinetic energy within this region, an observation which is at the origin of the rectifying behavior

[a]Electronic mail: toufik.sadi@iemn.univ-lille1.fr. URL: http://www.iemn.univ-lille1.fr/.

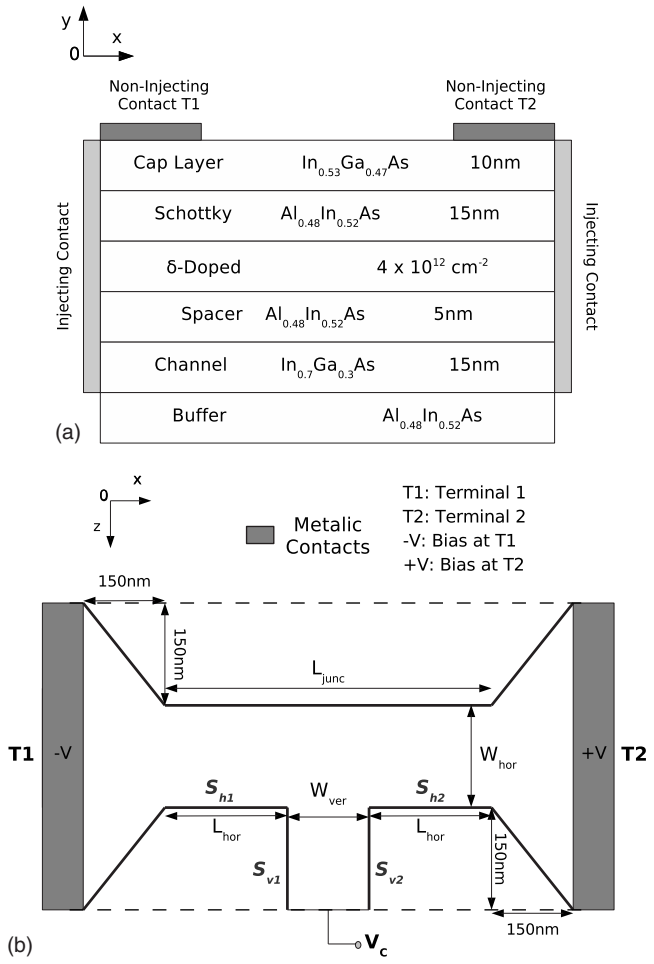

FIG. 1. Geometry and layer structure of the simulated TBJ. (a) shows a front view and (b) shows a top view of the simulated region. The semiconductor-air interfaces highlighted in (b) include a surface charge (σ), which is adjustable using the algorithm described below. In (b), W_{hor} and L_{hor} represent the width and length of the horizontal branch, respectively, and W_{ver} represents the width of the vertical branch. The sizes are: W_{hor} =120 nm, L_{hor}=150 nm, and W_{ver}=60 nm.

of a TBJ, as discussed in our previous publications. The relationship between rectification and quasiballistic transport in TBJs remains an unresolved issue; while several groups claim that the origin of the former effect is a direct consequence of the latter effect, other different groups reported observations of the rectifying behavior in junctions several times longer than the mean free path.[4] While the improved electron transport in the junction led to the common usage of the term "ballistic" to describe nanojunctions, electron transport in the devices is not always purely ballistic. Theoretical work suggests that nanojunctions in general can normally operate in the terahertz regime. This work does not only confirm the intrinsic capability of TBJs in the terahertz regime but also investigates the influence of surface charge effects on their HF behavior.

II. SIMULATED STRUCTURE

The device simulated in this work is a TBJ based on a δ-doped AlInAs/InGaAs heterostructure fabricated at the IEMN.[5] The structure is illustrated in Fig. 1, showing a front view and a top view of the device simulated region. The T-junction incorporates a main horizontal branch characterized by a width W_{hor} of 120 nm and a length L_{hor} of 150 nm, and a vertical branch characterized by a width W_{ver} of 60 nm. The Monte Carlo simulation domain is limited to a small region of the device located between the two contact terminals (T_1 and T_2) at both sides of the main branch. Electron transport outside this simulation domain is assumed to be near equilibrium. It is noteworthy that such structure also incorporates a third terminal (T_3) located at the end of the vertical branch.[5] In this analysis, the device is biased in a push-pull fashion, assuming an unbiased T_3 (i.e., with a floating potential). In such a case, the bottom of the vertical branch is considered to be open circuited. This biasing scheme allows the study of the rectifying behavior of the device by analyzing, for example, the variations in the output potential at the bottom end of this branch (V_C) with the applied bias.

III. SIMULATION METHOD

The Monte Carlo simulator self-consistently couples 3D electronic dynamics with a solution of 3D Poisson's equation. This simulator has been very well calibrated with experimental studies to provide reliable device predictions. Details and advantages of the simulation model over previously developed 2D models are thoroughly discussed in Ref. 7. As demonstrated in Ref. 7, the correct inclusion of the real device geometry in the 3D space is necessary for the accurate analysis of the microscopic properties of electron transport, which is important to understand the physics of these devices. The model minimizes significantly the need for parameter fitting to match experimental results and leads to more realistic macroscopic and microscopic characteristics. As discussed in Ref. 7, the surface charge σ at the surrounding surfaces of the simulated devices significantly influences electron transport,[12,13] since they are characterized by a relatively high-surface-to-volume ratio. The newly developed self-consistent charge model in Ref. 12 was implemented in our simulator to account for surface charge effects. Such model involves the dynamic adjustment of the surface charge according to the surrounding electron density. By allowing the surface charge to vary according to the neighboring electron distribution, more realistic depletion region widths are obtained. The use of a surface charge model fixing the value of such charge to the experimentally extracted equilibrium value has proved inefficient in structures with thin layers.[12] Such value may lead to full depletion of charge in such layers, which is not physically justified; in such a case, the surface states should not be susceptible to be occupied by free electrons, corresponding to a much lower σ.

To the authors' knowledge, theoretical work on HF simulations of nanojunctions employed the simple surface charge model, assuming a fixed charge density in all the device surfaces. As discussed above, such model is not reliable when studying devices based on thin branches. While the application of the self-consistent charge model for dc (static) studies of nanojunctions is straightforward, it needs to be adjusted for HF (dynamic) studies. To reduce the computational cost, the applied potentials at terminals T_1 (V_L)

and T_2 (V_R) are assumed to follow a squarewave form, with the same frequency f. In general, the biasing scheme is chosen such that push-pull polarization is maintained at every instant of the simulation. In the first half-period (case 1), V_L is set to $-V_1$ and V_R is set to $+V_1$, while in the second half-period (case 2), V_L is set to $+V_2$ and V_R is set to $-V_2$. The HF charge model is applied as follows. First, we perform dc simulations to determine the fixed charge distribution in each surface of the junction, for both biasing cases (we use σ_1 to define the charge density at a given surface for case 1, and σ_2 to define the charge density for case 2). Since little is known about the fixed charge at the surfaces (especially at high frequencies), we suggest three models for considering surface effects at these conditions. The first model (referred to as model I) allows instantaneous change of σ (from σ_1 to σ_2 or vice versa) with the applied potential. The second model (referred to as model II) allows a time-dependent change of σ by introducing the time constant concept. If a change in the applied potential occurs from case 1 to case 2 (or from case 2 to case 1), σ is given as follows:

$$\sigma = \begin{cases} \sigma_1 + [(\sigma_2 - \sigma_1) f(t)] & \text{from case 1 to case 2}, \\ \sigma_2 + [(\sigma_1 - \sigma_2) f(t)] & \text{from case 2 to case 1}, \end{cases} \quad (1)$$

where $f(t)$ is a time-dependent function given by

$$f(t) = 1 - \exp(-t/\tau) + \exp[-(T/2)/\tau]/2. \quad (2)$$

t is the time elapsed since the last potential change, τ is the time constant, and T is the time period. The third model (referred to as model III) sets the value of σ to the average value $(\sigma_1+\sigma_2)/2$. This represents the opposite case of Model I, since it does not allow time for surface charge change. Clearly, models I and III represent special cases of model II, corresponding to $\tau \sim 0$ and $\tau \sim \infty$, respectively.

As discussed in literature, the fixed charge density at the surfaces of the junction is dependent on electron dynamics at the vicinity of these surfaces, and hence on the applied potential, and the model developed in Ref. 12 is efficient in generating reliable dc results by accounting for such dependencies. The model developed here aims for a realistic inclusion of surface charge effects at high frequencies, by allowing for the variation in the local surface charge density with the varying applied potential. In general, the main parameter of Eq. (2) (τ) physically defines how fast surface charge responds to variations in the applied potential, from one biasing condition to another, with a higher τ signifying a slower response. For a device with a given τ, the influence of surface charge depends on the applied signal frequency (and hence the period T). At very high frequencies (corresponding to a relatively high τ/T), surface charge variations are expected to respond very slowly to potential variations, giving σ_1 and σ_2 values approaching their average values (model III). At relatively low frequencies (corresponding to a relatively low τ/T), there is enough time for the charge densities at different surfaces to reach their equilibrium values, giving σ_1 and σ_2 values approaching their dc values (model I). For a given device, τ is a parameter that can be extracted from calibration with HF experimental data. Its value may depend on several parameters, such as trap densities and electron trapping rates. At the HF regime considered in this work, the average lifetime of trapped electrons may be much larger than T, which may lead to the conclusion that model III may be most suitable for this study. Nonetheless, little is known about the trapping processes at the device surfaces, and therefore we need to investigate the effect of the time constant variation on the device performance.

To fully understand the electron dynamics in the simulated TBJ, we show in Fig. 2 the dc surface charge profiles at different surfaces of the junction. As can be seen, the average surface charge at the horizontal surface near the positively biased contact increases significantly with the increasing bias. This gives rise to the asymmetry in free charge density profiles in the channel which is at the origin of the rectifying behavior of a TBJ, as discussed below. Figure 2 shows that profiles of the surface charge at the vertical branch are more or less the same for biases considered in this work. This observation can be explained by the fact that this branch is nearly depleted of free electrons, since the branch is relatively thin (see Ref. 12 for more details). As thoroughly discussed in Ref. 7, our simulator has been carefully calibrated with reported dc experimental studies of nanojunctions. The surface charge at the free surfaces on top of the cap layer was set to a value of 5.0×10^{12} cm^{-2}, to obtain good agreement with the experimental results from the study of similar structures.[1] The simulations are run assuming an isothermal temperature distribution equal to the ambient temperature (300 K).

IV. RESULTS AND DISCUSSIONS

While the model described above is specifically designed for applied biases of a squarewave form, it allows reliable qualitative HF studies of surface charge effects on the performance of TBJs as voltage rectifiers. For the analysis of the TBJ considered in this work, we generate device simulation results at a relatively low frequency of 250 GHz and a relatively high frequency of 1 THz. For both frequencies, the three charge models described above are applied to demonstrate surface charge effects on the device HF performance. The biasing scheme is chosen such that push-pull polarization ($V_L=-V_R$) is satisfied in the first half-period. In the second half-period, both V_L and V_R are set to zero. This corresponds to $V_1=V$ and $V_2=0$ V. In the case of model II, three time constant (τ) values are used: $T/10$, $T/5$, and $5T$. Figures 3 and 4 show the variations in the average V_C for these frequencies and the three charge models, as well for the dc case. Separate results are shown for both half-periods (cases 1 and 2). In Figs. 5 and 6, we show the time dependence of V_C for the cases above, at a relatively high bias ($V=0.3$ V). Details of the V_C versus V curves vary for each surface charge model. The figures demonstrate how the choice of the charge model influences considerably the predicted results, especially at higher frequencies.

Results from the application of model I shows a strong time dependence of V_C. At high frequencies, the electron population does not have the time to readjust to the new surface charge values and hence does not settle to a steady state. This leads to unrealistic average V_C values below dc values in the first half-period and above the dc value in the

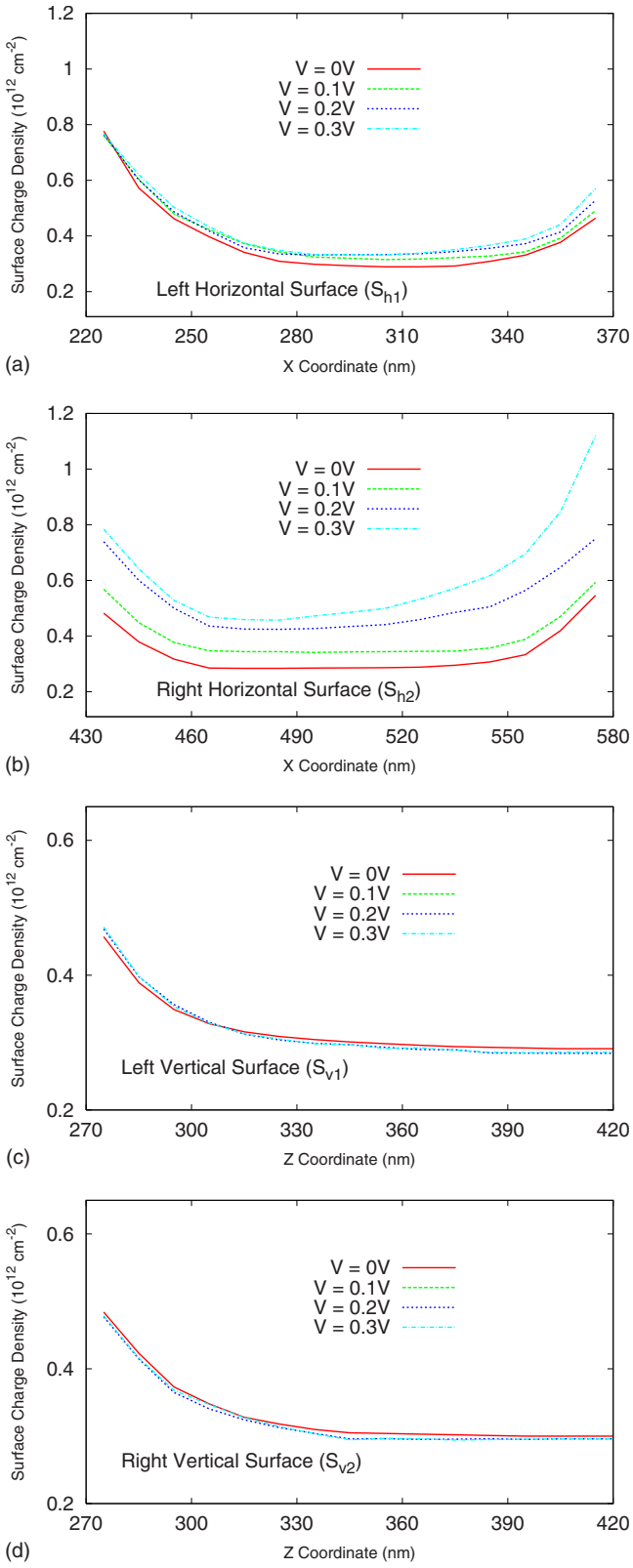

FIG. 2. (Color online) Static spatial profiles of fixed charge density at surfaces (a) S_{h1} (left horizontal surface at z=270 nm), (b) S_{h2} (right horizontal surface at z=270 nm), (c) S_{v1} (left vertical surface at x=370 nm), and (d) S_{v2} (right vertical surface at x=430 nm). The symbol used for each surface is indicated in Fig. 1. Results are shown for four different bias (V) values: 0, 0.1, 0.2, and 0.3 V.

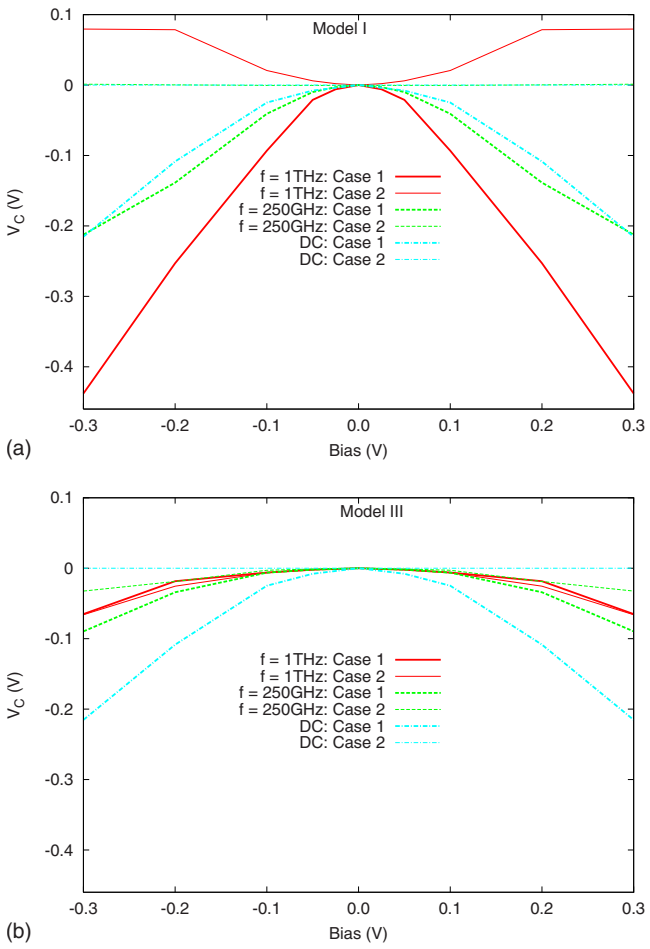

FIG. 3. (Color online) Variations in the average V_C with V, obtained from surface charge models I and III. The results are shown for frequencies 250 GHz and 1 THz, as well as for the dc case, and for both half-periods (cases 1 and 2).

second half-period. Model III shows a much less time dependence of V_C. The average V_C values are, in general, above dc values in the first half-period and below the dc value in the second half-period. While both models represent extreme cases of the influence of surface charge on the HF performance, model III may be more suitable at high frequencies since the surface charge is expected to respond very slowly to contact bias changes. At 1 THz, this model is shown to give results that are similar in both half-periods. This suggests that surface charge effects may be a dominant factor in determining the HF behavior of three-terminal junctions. Such possibility leads to an important conclusion: for an improved performance at high frequencies, future designs should incorporate a reduced junction length to minimize the influence of surface charge effects over electron transport and enhance the role of ballistic transport on the switching behavior of TBJs. Figures 3–6 illustrate how a progressive increase in τ, from 0 (model I) to ∞ (model III), seriously affects the details of the time response of V_C and its average values. While the influence of surface charge effects and quasiballistic transport on the TBJ rectifying behavior cannot be identified separately, the dependence of V_C on τ shown in Figs. 3–6 provides interesting information that can be used for calibration purposes. The study of such dependence allows the extraction of a set of parameters (such as the average V_C value or its peak instantaneous values) that can be

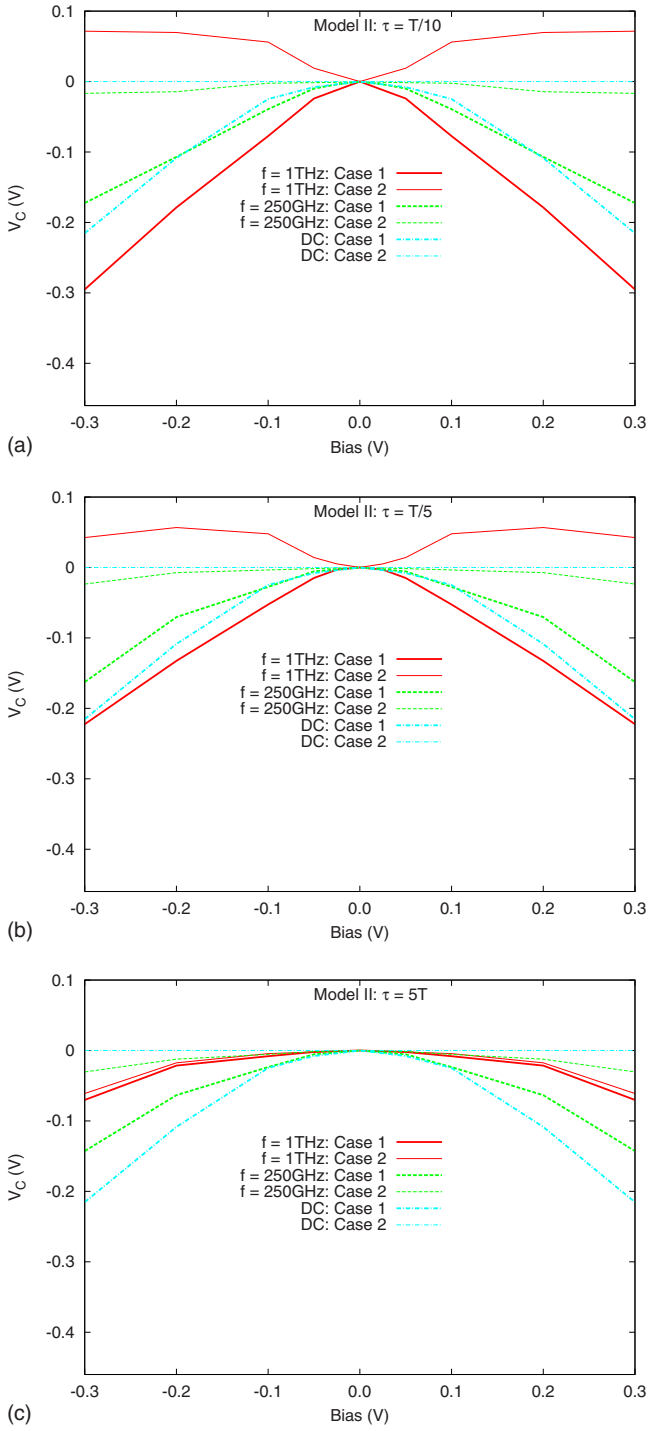

FIG. 4. (Color online) Variations in the average V_C with V, obtained from surface charge model II with three different τ values. The results are shown for frequencies 250 GHz and 1 THz, as well as for the dc case, and for both half-periods (cases 1 and 2).

used to determine the most suitable τ value giving good agreement with HF experimental data (which are unfortunately not available at the moment).

To explain the behavior of the TBJ observed in Figs. 3 and 4, we perform a microscopic analysis of the properties of electron transport in these nanodevices. For a deeper understanding of the physics governing device operation at high frequencies, we show in Figs. 7–9 the variation in the mean electron velocity in the x direction, energy, and density along

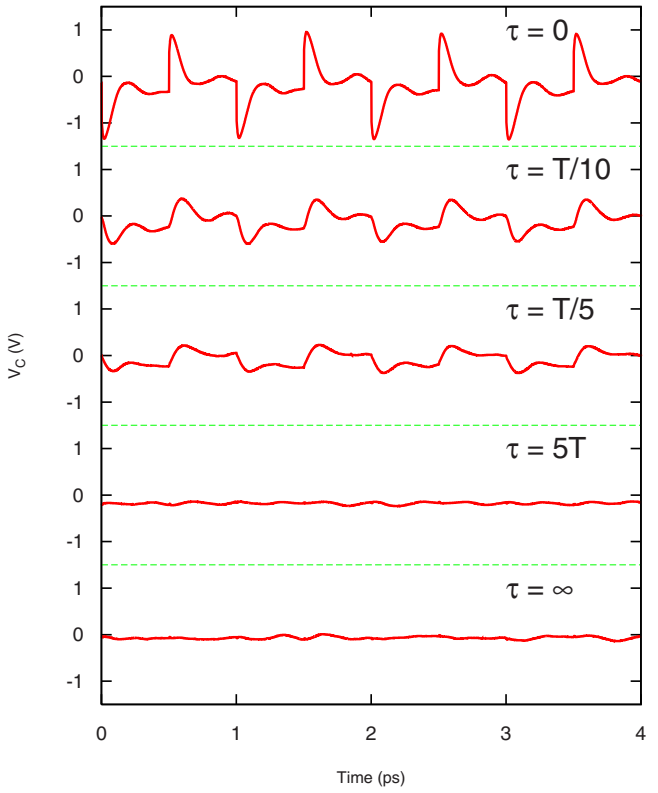

FIG. 5. (Color online) Variations in V_C with time for a frequency of 1 THz, obtained from models I and III, as well as model II with three different τ values. The results are for V=0.3 V.

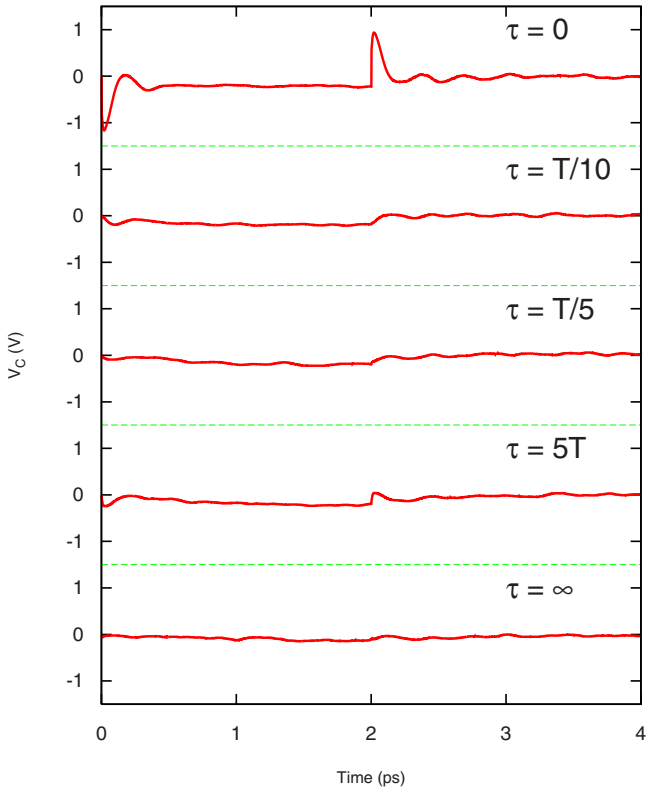

FIG. 6. (Color online) Variations of V_C with time for a frequency of 250 GHz, obtained from models I and III, as well as model II with three different τ values. The results are for V=0.3 V.

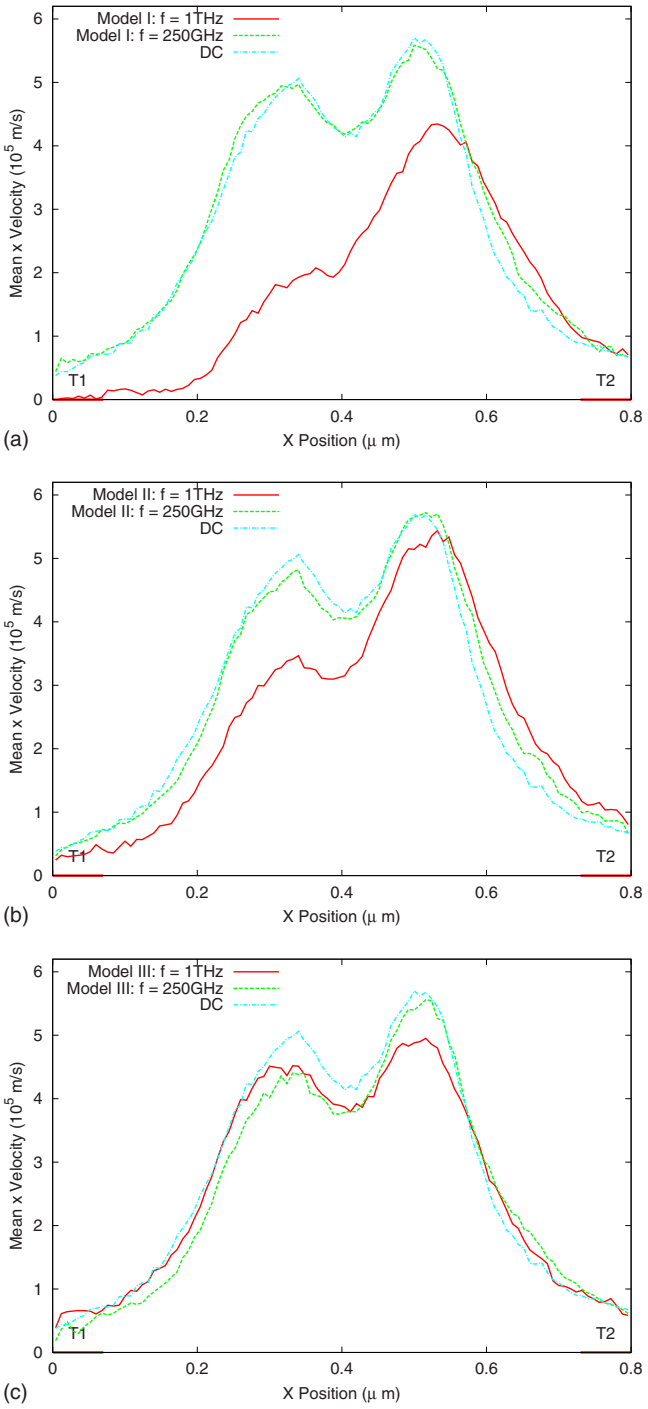

FIG. 7. (Color online) Variations in the mean electron velocity in the x direction in the channel at z=0.21 μm, for the dc case, a frequency of 250 GHz, and a frequency of 1 THz, and for surface charge models I (top curve), II (middle curve), and III (bottom curve). For model II, τ is set to $T/5$. The results are for a bias V of 0.3 V.

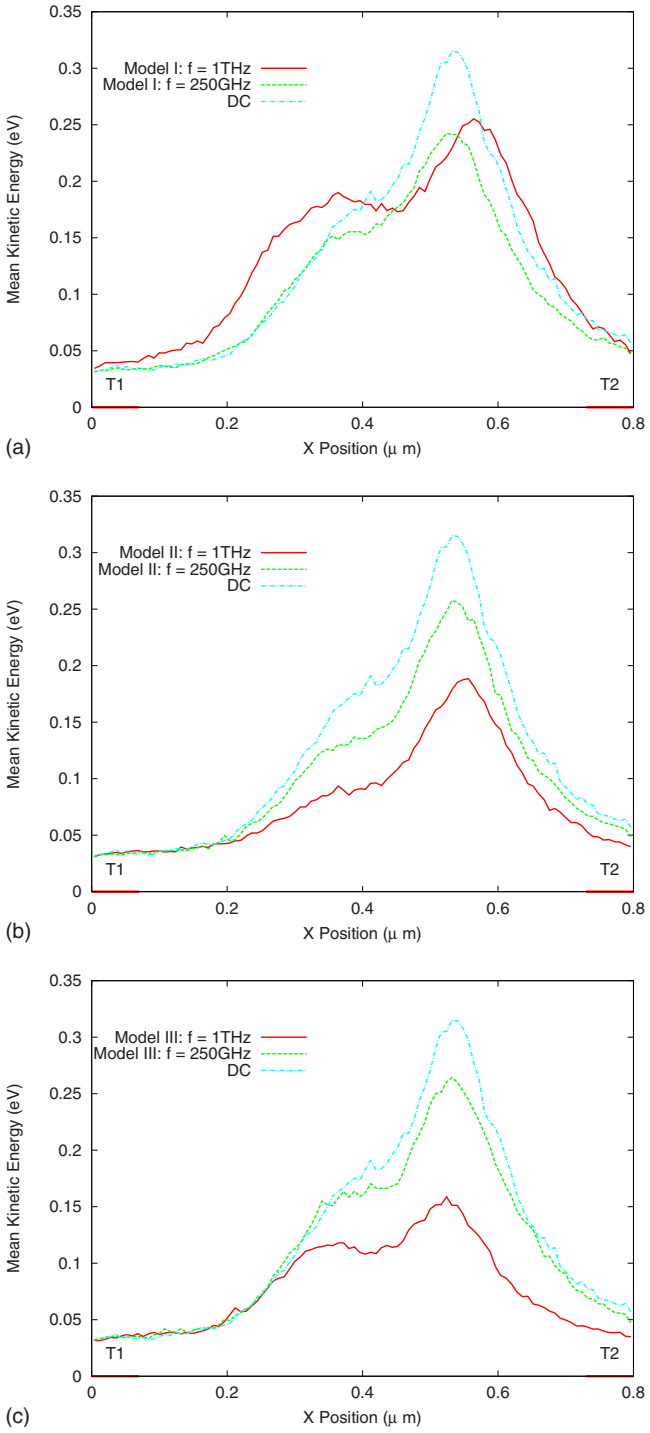

FIG. 8. (Color online) Variations in the mean electron kinetic energy in the channel at z=0.21 μm, for the dc case, a frequency of 250 GHz, and a frequency of 1 THz, and for surface charge models I (top curve), II (middle curve), and III (bottom curve). For model II, τ is set to $T/5$. The results are for a bias of 0.3 V.

the channel, respectively. The results are taken at the z coordinate (z_{HC}) corresponding to the middle of the device: z_{HC} =0.21 μm. These results are shown for the first-half period (V_L=$-V$, V_R=$+V$) for a relatively high bias. As discussed above, model I leads to unrealistic results, especially at high frequencies (f=1 THz). In this case, it has been verified that there exists a significant increase in electron transitions to the upper valleys, resulting in a significantly reduced average velocity. Analysis of the microscopic results obtained from models II (τ=$T/5$) and III ($\tau\sim\infty$) show the expected asymmetry in velocity, energy, and density, which is weakened at higher frequencies but also at higher τ values. The average (and peak) velocities and energies are also reduced at higher frequencies and τ values. The energy profiles, showing a constant increase in electron energy in the junction, are maintained at terahertz frequencies. These profiles, which are at the origin of rectifying behavior in three-terminal junc-

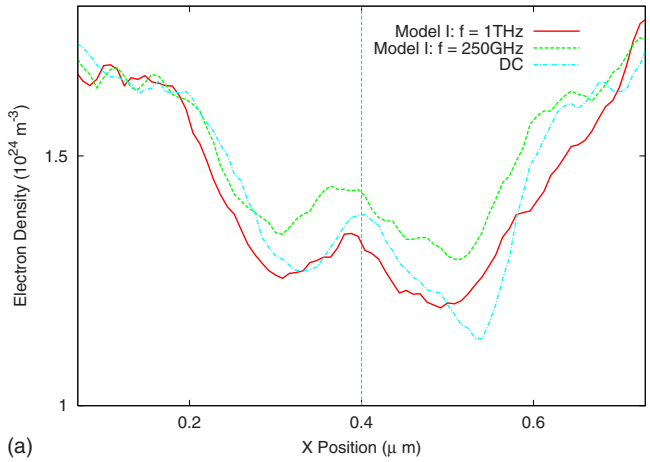

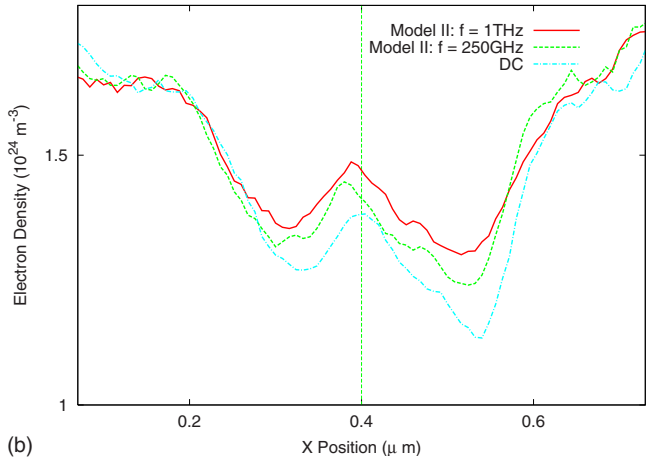

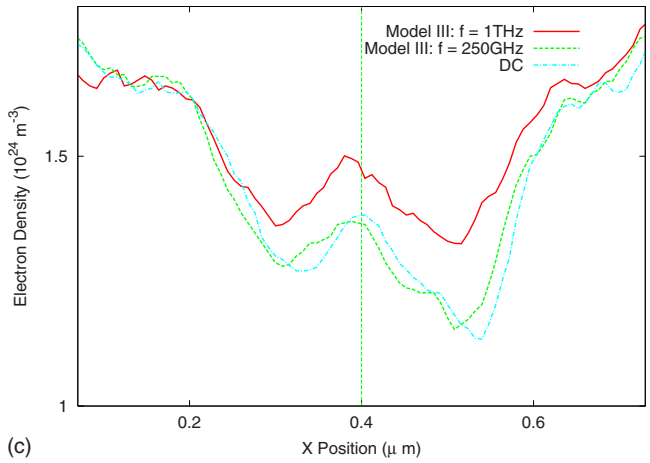

FIG. 9. (Color online) Variations in the mean electron density in the channel at $z=0.21$ μm, for the dc case, a frequency of 250 GHz, and a frequency of 1 THz, and for surface charge models I (top curve), II (middle curve), and III (bottom curve). For model II, τ is set to $T/5$. The results are for a bias of 0.3 V. The vertical line indicates the center of the device.

tions, lead to another important conclusion: such devices maintain their nonlinear behavior at very high frequencies and therefore are suitable for use in terahertz applications.

TBJs can be used as multiplexer/demultiplexers (MUX/DEMUXs) for logic applications. This is by biasing the third terminal at the bottom end of the vertical branch of the TBJ and introducing a Schottky gate contact, as explained in Ref. 7. Previous work on this structure consisted of applying a

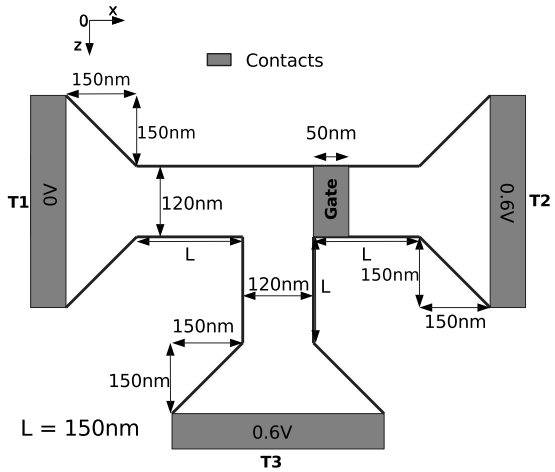

FIG. 10. Geometry of the simulated TBJ with a gate contact.

simple 2D Monte Carlo model for qualitative studies demonstrating the functioning of this structure (with an approximated geometry) at terahertz frequencies.[6] In this work, we consider the real 3D geometry, which is important for HF predictions, to confirm the device operation at these frequencies but also demonstrate the influence of surface charge effects. The structure is shown in Fig. 10. For this study, the following biasing scheme is used. The potential values at the three Ohmic contacts, *T1, T2, and T3*, are set to 0, 0.6, and 0.6 V, respectively. The applied gate potential (V_G) is assumed to follow a squarewave form, with a frequency f of 1 THz and magnitudes +0.75 and −0.75 V in the first and second half-periods, respectively. When V_G is negative most of the current flows through terminal T_3 (I_3), and when V_G is positive most of the current flows through terminal T_2 (I_2); this behavior explains its characteristic as a MUX/DEMUX.

Figures 11 and 12 show the variation in the current with time, for these biasing conditions, when using models I and II ($\tau=T/5$). This work presents a good opportunity to apply our 3D HF simulator to confirm observations obtained using the 2D model in Ref. 6, such as the fact that the MUX/DEMUX function is maintained at 1 THz, as shown in Figs. 11 and 12. However, it is important to note that results are quantitatively different, due to the neglect of 3D geometry features and the simple treatment of surface charge effects in the 2D model.[6] As can be observed, surface charge models give considerably different current profiles. The I_2 curves show strong peaks, as this quantity depends directly on the gate potential variations. For model I, the I_2 peak values are observed mostly at the start of each half-period, reflecting the instantaneous change in surface charge density. For model II, the I_2 peak values are observed roughly in the middle of each half-period, reflecting the evolution of surface charge density with time, according to Eq. (1). The effect of surface charge may be better studied by observing the variation of current through the vertical branch (I_3), where variations in V_G have a reduced direct influence. Analysis of the current time variations shows that the average I_3 is significantly affected by the choice of the charge model. The application of model I results in relatively less fluctuations in the I_3 curve, with the expected strong peak observed at the

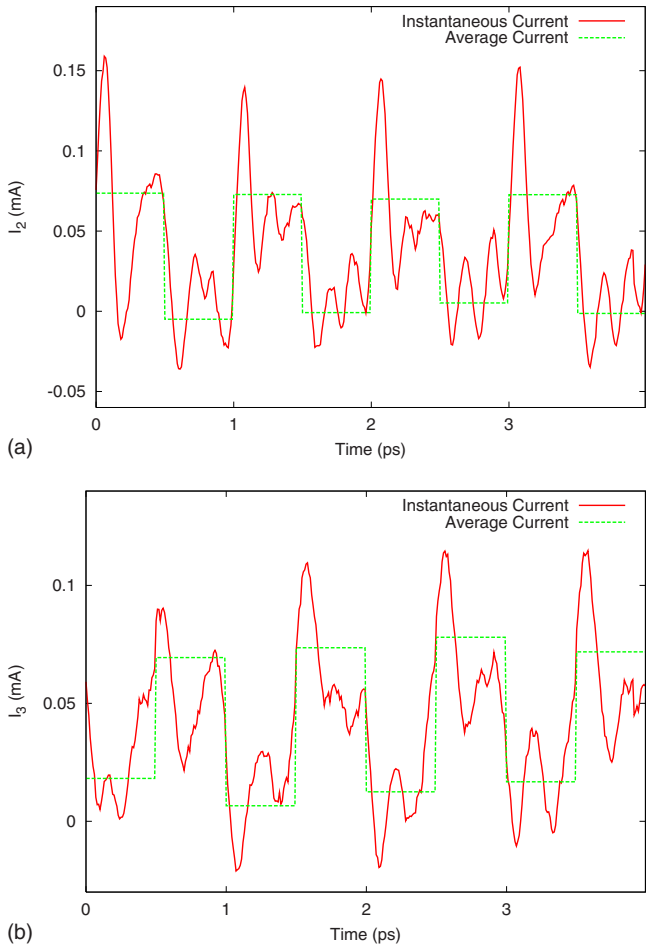

FIG. 11. (Color online) Time variation of the device currents for a 1 THz frequency and surface charge model I. The top graph shows the current through the right branch (I_2), and the bottom graph shows the current through the vertical branch (I_3).

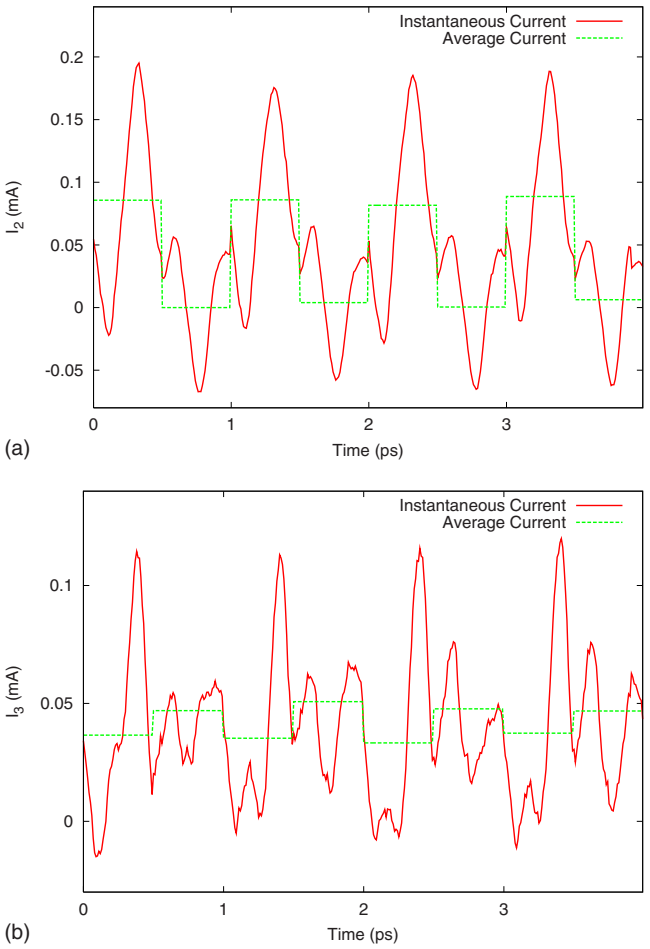

FIG. 12. (Color online) Time variation of the device currents for a 1 THz frequency and surface charge model II ($\tau = T/5$). The top graph shows the current through the right branch (I_2), and the bottom graph shows the current through the vertical branch (I_3).

start of each half-period. In this case, when V_G changes from +0.75 to −0.75 V, the new relatively high-surface charge values (at the vertical branch) give a visible decrease in I_3 from the peak value, before settling at lower values for the rest of the half-period. When V_G changes from −0.75 to +0.75 V, the new relatively low-surface charge values (at this branch) give a visible increase in I_3 from the minimum value, before settling at higher values for the rest of the half-period. The time variation of surface charge density when using model II gives more complex I_3 profiles, with several visible peaks and minima occurring at the same half-period. This part of the study is another practical example demonstrating the importance of understanding surface charge effects for a complete understanding of the behavior of nanojunctions at high frequencies.

V. CONCLUSION

This paper presents a theoretical study of the intrinsic performance of three-terminal junctions based on InGaAs/InAlAs heterostructures at high frequencies, using a 3D Monte Carlo simulator. As well as analyzing the basic output characteristics of the nanostructure, the influence of surface charge effects, considered using more realistic models, on the switching behavior and the properties of electron transport is shown. The results demonstrate how the behavior of the devices as switches is sustained at the terahertz frequency range, and most importantly illustrates the role played by surface charge effects in this regime. It is suggested that optimum future designs should include shorter junctions; a reduced-size junction would enhance the role of ballistic transport over the role of surface charge effects and further extend the device operation in the terahertz regime. While this work demonstrates how TBJs can operate in the terahertz frequency range, experimental studies of fabricated three-terminal junctions reported cutoff frequencies much less than the theoretically predicted ones (see, for example, Ref. 14). This is mainly due to extrinsic cross-talk capacitances and access resistances. This means that care has to be devoted to the optimization of bonding pads geometry and the minimization of parasitic extrinsic effects.

ACKNOWLEDGMENTS

The authors would like to thank F. Dessenne and Y. Roelens from the IEMN for valuable discussions.

[1]T. Gonźalez, I. Iñiguez-de-la-Torre, D. Pardo, J. Mateos, S. Bollaert, Y. Roelens, and A. Cappy, Phys. Status Solidi C **5**, 94 (2008).
[2]S. Bollaert, A. Cappy, Y. Roelens, J. S. Galloo, C. Gardes, Z. Teukam, X.

Wallart, J. Mateos, T. Gonzalez, B. G. Vasallo *et al.*, Thin Solid Films **515**, 4321 (2007).
[3]L. Bednarz, Rashmi, P. Simon, I. Huynen, T. Gonźalez, and J. Mateos, IEEE Trans. Nanotechnol. **5**, 750 (2006).
[4]D. Wallin, I. Shorubalko, H. Q. Xu, and A. Cappy, Appl. Phys. Lett. **89**, 092124 (2006).
[5]J. S. Galloo, E. Pichonat, Y. Roelens, S. Bollaert, X. Wallart, A. Cappy, J. Mateos, and T. Gonźales, Proceedings of the International Conference on Indium Phosphide and Related Materials '04, 2004 (unpublished), p. 378.
[6]J. Mateos, B. G. Vasallo, D. Pardo, T. Gonźales, J. S. Galloo, Y. Roelens, S. Bollaert, and A. Cappy, Nanotechnology **14**, 117 (2003).
[7]T. Sadi, F. Dessenne, and J.-L. Thobel, J. Appl. Phys. **105**, 053707 (2009).
[8]I. Shorubalko, H. Q. Xu, I. Maximov, P. Omling, L. Samuelson, and W. Seifert, Appl. Phys. Lett. **79**, 1384 (2001).
[9]H. Q. Xu, Appl. Phys. Lett. **80**, 853 (2002).
[10]H. Q. Xu, I. Shorubalko, D. Wallin, I. Maximov, P. Omling, L. Samuelson, and W. Seifert, IEEE Electron Device Lett. **25**, 164 (2004).
[11]L. Worschech, D. Hartmann, S. Reitzenstein, and A. Forchel, J. Phys.: Condens. Matter **17**, R775 (2005).
[12]I. Iñiguez-de-la-Torre, J. Mateos, T. Gonźalez, D. Pardo, J. S. Galloo, S. Bollaert, Y. Roelens, and A. Cappy, Semicond. Sci. Technol. **22**, 663 (2007).
[13]A. M. Song, M. Missous, P. Omling, I. Maximov, W. Seifert, and L. Samuelson, Appl. Phys. Lett. **86**, 042106 (2005).
[14]L. Bednarz, Rashmi, G. Farhi, B. Hackens, V. Bayot, I. Huynen, J. S. Galloo, Y. Roelens, S. Bollaert, and A. Cappy, Proceedings of the 35th European Microwave Conference '05, 2005 (unpublished), p. 4.